

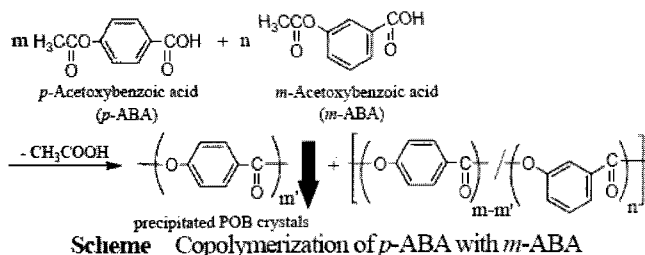
Composition Control of Aromatic Copolyester by means of Controlling Shear Flow

Toshimitsu Ichimori*(市森俊充), Shinichi Yamazaki (山崎真一), and Kunio Kimura (木村邦生)

Graduate School of Environmental Science, Okayama University, 3-1-1 Tsushima-naka, Kita-ku, Okayama 700-8530 JAPAN, E-mail polykim@cc.okayama-u.ac.jp

INTRODUCTION

Precise control of polycondensation is of academic and industrial importance to create new polymer materials. Many attractive reactions have been recently developed, such as synthesis of sequence-defined polymers¹, condensative chain polymerization², solid-state polycondensation³, nucleation-elongation polymerization^{4,5}, and fractional polycondensation^{6,7}. Fractional polycondensation may be defined as a polymerization in which certain monomers are selectively incorporated into the copolymerization system. Copolymers rich in a *p*-oxybenzoyl moiety were synthesized from the copolymerization of *p*-acetoxybenzoic acid (*p*-ABA) and *m*-acetoxybenzoic acid (*m*-ABA) by using selective crystallization of oligomers during polymerization as depicted in Scheme.



Numerous studies have been reported on phase separation of polymer solution under shear flow from the 1960s. Many researchers were particularly attracted by the long string-like structures of flexible polymers, called the “shish-kebab” structure, obtained from the stirred solution⁸⁻¹⁰. It had been pointed out that the molecular orientation was induced by shear flow, and it was crucial for formation of the fibrous crystals¹¹. With respect to rigid-rod polymers, studies on shear-induced polymer chain orientation and morphology have been done on poly(ether ether ketone)¹² and liquid crystalline polymers¹³. Rigid-rod polymers easily align with the shear flow direction depending on the axial aspect ratio. Polymer molecules elongated by the shear flow coagulated easily to form the nuclei due to the entropic advantage, and then polymer molecules aligned by the shear flow crystallized effectively to form the crystals^{9,10}.

Orientation of the molecules plays an important role for the reaction rate in solution polymerization as well. Previous kinetic studies for solution polymerization of rigid-rod polymers showed that the rate constant decreased by an order of magnitude after an initial period, and the molecular weight increased very slowly with time^{14,16}. The decrease in the reaction rate was attributed to rotational diffusion limitations when the molecules became long enough¹⁵⁻¹⁷. In the semidilute solution, the rotational diffusivity decreased sharply with molecular length, and the rate of generation of molecular pairs, which satisfied the criteria for reaction, became very slow.

These previous studies imply that the selectivity of the *p*-oxybenzoyl moiety prepared by fractional polycondensation is likely influenced by shear flow, and the composition of aromatic copolymers can be consequently controlled by hydrodynamically induced phase separation. In this study, we examined the influence of shear flow on the selective preparation of poly(*p*-oxybenzoyl) (POB) and the composition control of copolymers in the polymerization of *p*-ABA and *m*-ABA by means of controlling shear flow.

EXPERIMENTAL

Materials

The *p*-ABA and *m*-ABA were purchased from TCI Co. Ltd. and Aldrich Co. Ltd., respectively. They were purified by recrystallization from ethyl acetate. Liquid paraffin (LPF) was purchased from Nacalai Tesque, Co. Ltd., and purified by vacuum distillation (220-240°C/0.3 mmHg). Phenyl 4-[4-(benzoyloxy)benzoyloxy]benzoate (PPPP) and phenyl 4-[3-(benzoyloxy)benzoyloxy]benzoate (PMPP) were synthesized as oligomer model compounds according to the previous procedures^{18,19}.

Measurements

Morphology of the polymer crystals was observed on a Hitachi S-3500N scanning electron microscope (SEM). Samples for SEM observation were dried, sputtered with gold, and observed at 20 kV. Infrared (IR) spectra were measured on a JASCO FT/IR-410 spectrometer. A wide-angle X-ray scattering (WAXS) pattern was measured on a Rigaku Gaijer Flex with nickel-filtered Cu K α radiation (35 kV, 20 mA). NMR spectra were recorded on a JEOL AL300 SC-NMR at 300 MHz (^1H).

Polymerization

Typical polymerization method under shear flow is as follows. *p*-ABA (0.45g, 2.5 mmol), *m*-ABA(0.45g, 2.5 mmol) and LPF (60 mL) where χ_f was 50 mol% were placed into a cylindrical vessel equipped with a mechanical stirrer and a gas inlet tube. The stir bar was a rod type, of which the diameter was 2.8 cm and the clearance between the inner wall of the cylindrical vessel and stir bar was 0.3 cm. The reaction mixture was heated under a slow stream of nitrogen up to 330°C with stirring speed of 1000 rpm. The temperature was maintained at 330°C for 6 h. The precipitates were collected by vacuum filtration at 330°C and washed with *n*-hexane and acetone.

Determination of the Content of *m*-Oxybenzoyl Moiety in Precipitates

A polymer sample (10 mg) and 1mL of 0.7 wt % KOH in methanol solution were placed in a test tube and kept at 25°C for 24 h until the sample was completely hydrolyzed. The solution was neutralized with dilute hydrochloric acid and then analyzed by using a Shimadzu GC-14B gas chromatograph with FID equipped with a Thermon-3000 (60-80 mesh) packed column. The content of *m*-oxybenzoyl moiety was calculated as the molar ratio of *p*-hydroxybenzoic acid and *m*-hydroxybenzoic acid. The values of χ_f and χ_p were calculated as follows:

$$\chi \text{ (mol \%)} = [m\text{-oxybenzoyl moiety}] / \{[p\text{-oxybenzoyl moiety}] + [m\text{-oxybenzoyl moiety}]\}$$

where χ_f and χ_p stand for the content of *m*-ABA in feed and that of *m*-oxybenzoyl moiety in the precipitate, respectively.

Kinetic Study

The *p*-ABA and *m*-ABA (0.90 g, 5.00 mmol) and LPF (60 mL) were placed into a cylindrical vessel equipped with a gas inlet and outlet tubes and a mechanical stirrer, which was the same apparatus used for the polymerization. The mixture was heated in an oil bath to 330°C with stirring under a slow stream of nitrogen. Acetic acid produced by the polymerization was trapped in the water. The amount of acetic acid produced, at a given time, was determined by titration with 0.1 M NaOH. The reactions obeyed second-order kinetics. The rate constants (k_2) were estimated from a extent of reaction plot (p) of evolved acetic acid as a function of polymerization time.

Preparation of Concentration-Temperature Phase Diagrams of Oligomer Model Compounds

Oligomer model compound PPPP and LPF were put into a cylindrical vessel equipped with a mechanical stirrer at different concentrations. They were placed into an oil bath and heated until the oligomer model was entirely dissolved with stirring. Then temperature was gradually lowered at a cooling rate of 5°C/h under stirring with a rod-type bar. The cloud point temperature was determined to prepare concentration-temperature phase diagrams.

RESULTS AND DISCUSSION

Polymerizations of *p*-ABA or *m*-ABA were carried out at 330°C in LPF for 6 h at 1.0% concentration. In this study, the polymerization concentration was described as the ratio of the theoretical polymer weight and the solvent volume. The reaction solution was stirred at speed of 300 and 1000 rpm, corresponding to shear rate ($\dot{\gamma}$) of 147 and 498 s $^{-1}$. Both *p*-ABA and *m*-ABA were not insoluble in LPF at room temperature, but they dissolved during reaction at heating up to 330°C. The solution became turbid within 20 min after the temperature reached

330°C due to the precipitation of oligomers followed by polymer precipitation after 6 h.

The shear flow and χ_f significantly influenced the morphology of the precipitated polymers as shown in Figure 1. The needlelike crystals were formed even by the copolymerization without shearing, when χ_f was up to 30 mol %^{6,7}. Although the fibrillated needlelike crystals were formed in the polymerization of *p*-ABA at γ of 147 s⁻¹, lathlike crystals or precipitates showing unclear morphology were observed under shear flow.

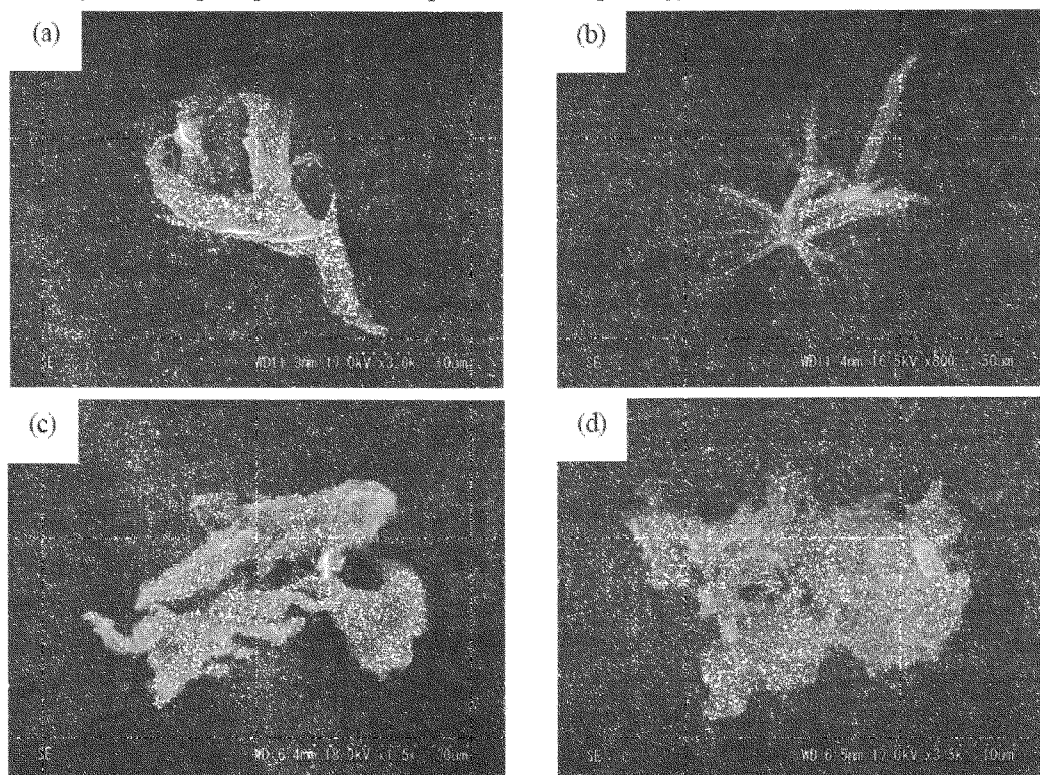


Figure 1. Morphology of the precipitated polymers prepared for 6 h: (a) $\chi_f=0$ mol %, $\gamma=489$ s⁻¹. (b) $\chi_f=0$ mol %, $\gamma=147$ s⁻¹. (c) $\chi_f=50$ mol %, $\gamma=489$ s⁻¹. (d) $\chi_f=50$ mol %, $\gamma=147$ s⁻¹.

The precipitated polymers did not uniformly cover the surface of the stir bar or the inner wall of the cylindrical reaction vessel. The deposition preferentially occurred at specific places, and the concentric rotating rings of the precipitated polymers appeared periodically as shown in Figure 2. The appearance of striations indicates the secondary flow pattern present in the stirred solution, which are generated by Taylor vortices in the solution. The polymers deposited on the sites on the stirring bar and the vessel wall where the two vortices collide. This means that the striations from two Taylor vortices rotating in opposite directions settled at the same place on the stirring bar and inner vessel wall. The purely laminar flow in the cylindrical vessel at low stirring speeds changed the Taylor vortices, bringing about a huge concentration of oligomers along the circular flow. Taylor vortices prevent the crystal growth, leading to the damage of the morphology of the precipitates.

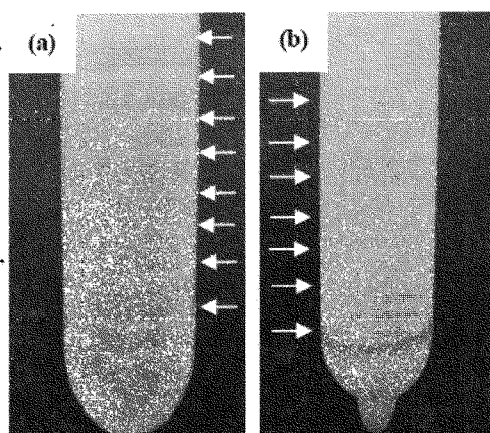


Figure 2. Photographs of (a) a reaction vessel and (b) a stirring bar showing preferential deposition of polymer crystals polymerized for 6 h at γ of 489 s⁻¹.

WAXS intensity profiles of the precipitates prepared under various conditions are shown in Figure 3. The diffraction peaks of POB prepared at 489 s⁻¹ were quite sharp and assigned according to the POB crystal unit cell^{20,21}. With the increase in χ_f , the diffraction peaks attributed to the POB crystal became broader and relative intensity of the broad halo from the amorphous region increased. It is well-known that the copolymerized moiety lowers the crystallinity due to the irregular sequence. The crystallinity was also influenced by shear flow, and it became lower with the increase of γ . The precipitated polymers prepared at χ_f of 50 mol %

and γ of 489 s^{-1} were almost amorphous.

These precipitates were insoluble in solvents, and thereby polymer structures could not be investigated by ^1H and ^{13}C NMR. They were confirmed by IR spectroscopy. Figure 4 shows IR spectra of the precipitates prepared under various conditions. In all spectra, a carbonyl band from the ester linkage appeared at 1739 cm^{-1} , and the characteristic bands from the carboxyl group and acetoxy group in monomers completely disappeared. These results confirm the formation of a high molecular weight polyester. The bands corresponding to the 1,3-phenylene moiety were observed at 1485 and 1415 cm^{-1} in the spectra of the precipitates prepared at χ_f of 20 and 50 mol %. The intensity of these bands increases with χ_f and the *m*-oxybenzoyl moiety is slightly copolymerized.

The yields and χ_p of the precipitated polymers are plotted as a function of χ_f as shown in Figure 5. The polymers were obtained as precipitates at χ_f of 0–30 mol % with the yield of 39.0–44.5% without shear flow. The polymerization at χ_f of 40 mol % did not afford any precipitates. At γ of 147 s^{-1} the polymers were precipitated at χ_f of 0–50 mol % with the yield of 26.3–40.2%. At higher γ of 489 s^{-1} the polymers were formed at χ_f of 0–50 mol % with the yield of 29.1–37.0%. Precipitation did not occur at χ_f of 60 mol % at γ of 147 and 489 s^{-1} . The yield of the precipitated polymers is inclined to become lower with the increase in γ . With respect to χ_p , those prepared at χ_f of 20 and 30 mol % were 5.3 and 12.3 mol % without shear flow. At γ of 147 s^{-1} the values of χ_p of the precipitates prepared at χ_f of 20, 40, and 50 mol % were 3.1, 13.3, and 31.6 mol %, respectively. At higher γ of 489 s^{-1} the values of χ_p of the precipitates prepared at χ_f of 20, 40, and 50 mol % were 2.3, 8.9, and 10.8 mol % respectively. The critical χ_f to induce the precipitation becomes higher by shear flow. The values of χ_p are much lower than those of χ_f and they decrease with the increase in γ . The *m*-oxybenzoyl moiety was hardly contained in the precipitates under shear flow, and the obtained polymers were mainly composed of a *p*-oxybenzoyl moiety.

Reaction-induced phase separation of oligomers in a poor solvent can be described on the analogous concentration–temperature phase diagram to that of partially miscible polymer solvent^{22–24}. The phase separation curve in the repulsive system in which there is no attractive interaction between oligomers and solvents is written as the combination of the freezing point curve of oligomers and the upper critical solution temperature (UCST) type dissolution curve. The mechanism of the fractional polycondensation between *p*-ABA and *m*-ABA has been revealed on the basis of this phase diagram as

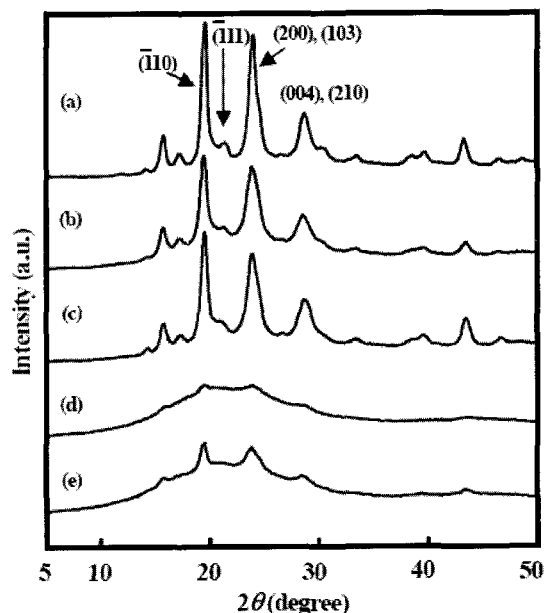


Figure 3. WAXS intensity profiles of the precipitates polymerized for 6 h: (a) $\chi_f=0$ mol %, $\gamma=489\text{ s}^{-1}$; (b) $\chi_f=20$ mol %, $\gamma=489\text{ s}^{-1}$; (c) $\chi_f=20$ mol %, $\gamma=147\text{ s}^{-1}$; (d) $\chi_f=50$ mol %, $\gamma=489\text{ s}^{-1}$; and (e) $\chi_f=50$ mol %, $\gamma=147\text{ s}^{-1}$.

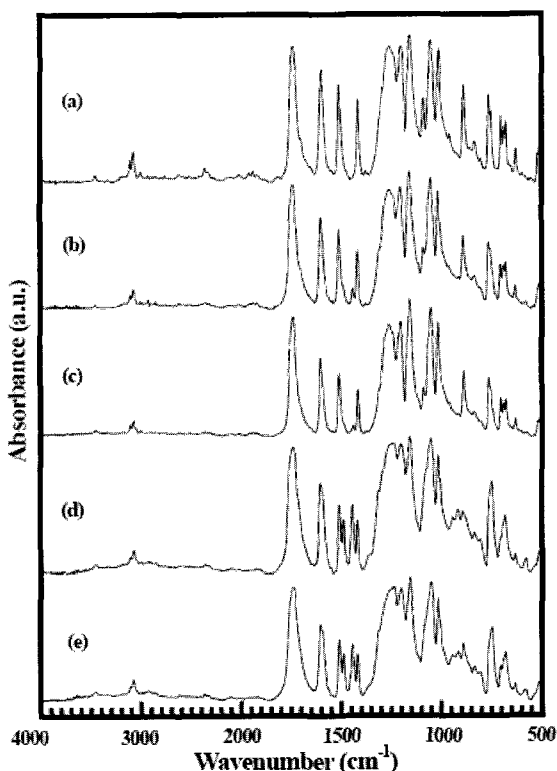


Figure 4. IR spectra of the precipitates polymerized for 6 h: (a) $\chi_f=0$ mol %, $\gamma=489\text{ s}^{-1}$; (b) $\chi_f=20$ mol %, $\gamma=489\text{ s}^{-1}$; (c) $\chi_f=20$ mol %, $\gamma=147\text{ s}^{-1}$; (d) $\chi_f=50$ mol %, $\gamma=489\text{ s}^{-1}$; and (e) $\chi_f=50$ mol %, $\gamma=147\text{ s}^{-1}$.

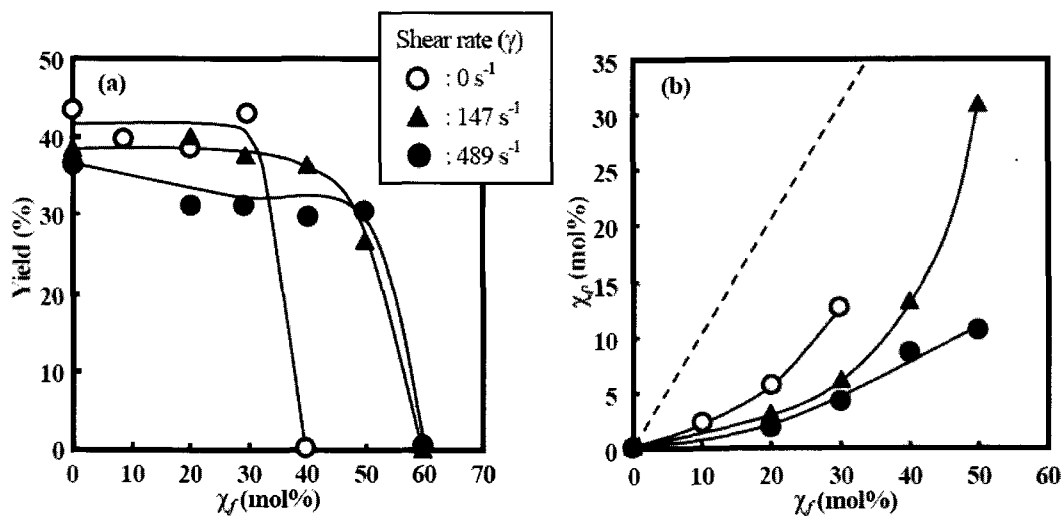


Figure 5. Plots of (a) yield and (b) χ_p of precipitated polymers as a function of χ_f at γ of 0, 147, and 489 s^{-1} .

follows⁶: *p*-Oxybenzoyl homo-oligomers are more rapidly formed in the solution than co-oligomers due to the difference in the reactivity of monomers. When the DP_n of the *p*-oxybenzoyl homo-oligomers exceeds a critical value, they are precipitated via crystallization to form the crystals at the early stage in the polymerization. Co-oligomers are gradually formed, and then they are also phase-separated. While co-oligomers containing a few *m*-oxybenzoyl moieties are precipitated via crystallization, they are excluded from the crystal by the segregation effect, and the *m*-oxybenzoyl moiety is not present in the crystals. At the middle stage of the polymerization, co-oligomers containing more *m*-oxybenzoyl moiety are formed in the solution, but they are unable to precipitate due to higher miscibility. Further polycondensation proceeds between oligomers in the precipitated crystals, and the POB crystals are finally formed. The fractional polycondensation is caused by the difference in the reactivity of monomers and in the phase separation behavior of the oligomer.

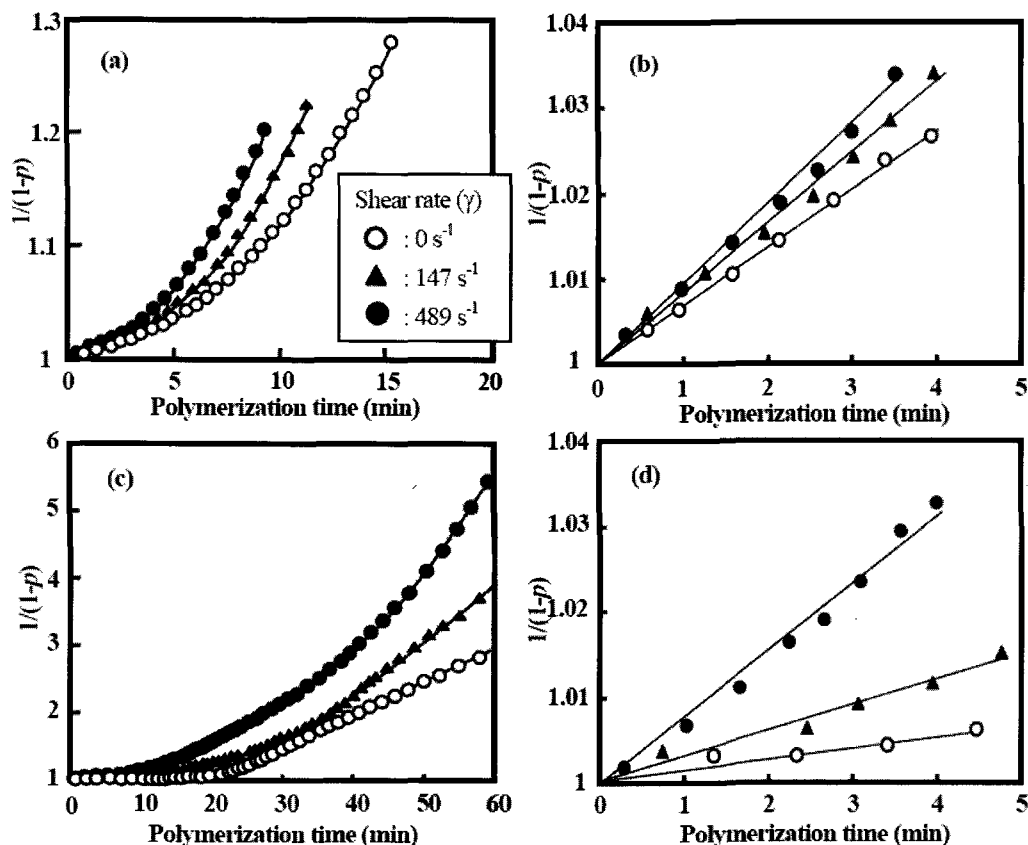


Figure 6. Kinetics of polymerization (a, b) *p*-ABA and (c, d) *m*-ABA in LPF at γ of (○) 0, (▲) 147, and (●) 489 s^{-1} . Initial concentration was $8.33 \times 10^{-2} \text{ mol L}^{-1}$.

First, the influence of shear flow on the reactivity of *p*-ABA and *m*-ABA was kinetically investigated. Figure 6 shows the plots of $1/(1-p)$ as a function of polymerization time under shear flow. Here, p is the extent of reaction. The reaction rate oppositely increases with time irrespective of shear rate as shown in Figure 6a, c. The rotational diffusivity, depending on the low molecular weight length, was not significantly influenced in the low molecular weight region, and it may be attributed to the concentration fluctuation. In a poor solvent, the phase separation is induced by the progress of polymerization, and the phase separation can be recognized as a process to enhance the local concentration of oligomers. The reaction rate might increase with time because of the increase in the concentration fluctuation caused by phase separation. With respect to shear rate, the reaction rate increases with an increase in the shear rate in both polymerization systems. At the very initial stage of polymerization, self-condensation reactions of *p*-ABA and *m*-ABA obeyed secondary ordered kinetics as shown in Figure 6b, d, and the reaction constants (k_2) at 330°C in LPF under shear flow were estimated as summarized in Table 1. Relative reactivity ratios of *p*-ABA to *m*-ABA were 3.3, 2.8, and 1.2 at γ of 0, 147, and 489 s^{-1} , respectively. Although the values of k_2 for both monomers increase with shear rate, the difference in the reactivity between *p*-ABA and *m*-ABA became smaller with the increase in γ . The increase in k_2 of *m*-ABA with shear rate was larger than that of *p*-ABA. Therefore, this might be due to the enhancement of the concentration in the collision inside the Taylor vortices rather than the orientation of molecules. Shear flow reduces the difference in the reactivity being undesirable to form the *p*-oxybenzoyl homo-oligomers.

Table 1. Second-order kinetic constants under various shear rates^a

Monomer	Shear rate [s^{-1}]	k_2 [$L mol^{-1} min^{-1}$]	DPn ^b	Ratio of k_2 ^c
<i>p</i> -ABA	0	0.10	1.28	3.3
	147	0.14	1.23	2.8
	489	0.16	1.22	1.2
<i>m</i> -ABA	0	0.03	- ^d	-
	147	0.05	-	-
	489	0.13	-	-

^a Initial concentration of *p*-ABA and *m*-ABA was $8.33 \times 10^{-2} mol \cdot L^{-1}$.

^b DPn of oligomers when the solution became turbid.

^c $k_2(p\text{-ABA})/k_2(m\text{-ABA})$

^d Not precipitated

Miscibility between the oligomer and the solvent as an effective parameter, and the influence of shear flow on the miscibility was examined. The phase-separated oligomers could not be isolated from the polymerization solution. The consolution curve and the freezing point curve of the phase-separated oligomer could not be accurately determined. In this study, relative locations of these curves are discussed on the basis of the miscibility of oligomer model compounds and LPF. Two kinds of compounds, PPPP and PMPP, were synthesized as the model compounds for homo-oligomer and co-oligomer, respectively. These compounds were end-capped by a phenyl group to avoid the further polymerization during the preparation of phase diagrams. The concentration-temperature phase diagrams of these oligomer model compounds and LPF were prepared at γ of 0, 147, and 489 s^{-1} by cloud-point measurements. In the diagrams as shown in Figure 7, the phase separation curves appeared as the combination of the freezing point curve and the UCST-type consolution curve as predicted. The phase separation curves of PMPP shifted toward lower temperature than that of PPPP. This result reveals that homo-oligomers of *p*-oxybenzoyl moiety possess the lowest critical concentration and critical molecular weight for phase separation. The freezing point curve of PPPP at $> 5 mol\%$ concentration where γ were 147 and 489 s^{-1} is located at lower temperature with respect to the influence of shear flow. However, it shifts toward higher temperature at a very low concentration ($< 1.0\%$), which is close to the real polymerization concentration of 1.0%. It is well-known that the solutions become turbid because of the shear-induced liquid-liquid phase separation or the enhancement of concentration fluctuations when semidilute polymer solutions are subjected to shear flow²⁵⁻³². The shear-induced phase separation is theoretically explained on the basis of the relaxation of elastic free energy of polymer chains under shear flow³³⁻³⁶. When the shear rate is larger than maximum relaxation rate, the excess elastic free energy built up in the solution by the deformation of the entangled polymer chains cannot be relaxed by disentanglements but can be released only by squeezing solvent. This solvent squeezing process results in the enhancement of concentration fluctuation and phase separation under shear flow. The theory suggests that the dynamical asymmetry between LPF chains and oligomers is crucial for the shear-induced phenomenon in the present study. LPF chain has mobility much smaller than the oligomer so that the latter relaxes much faster. As a

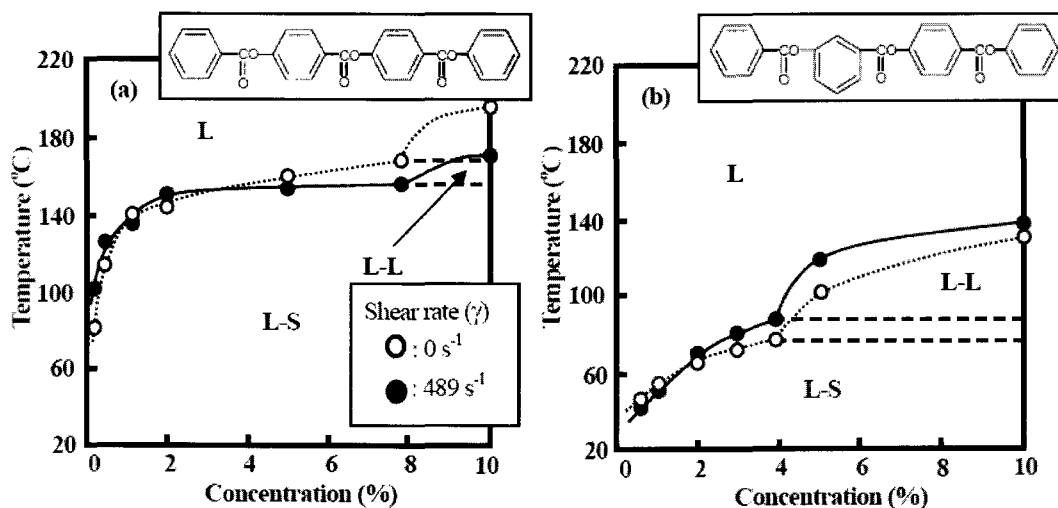


Figure 7. Concentration–temperature phase diagrams of (a) PPPP and (b) PMPP in LPF under shear flow at $\dot{\gamma}$ of (○) 0 and (●) 489 s⁻¹. L = homogeneous liquid phase, L–L = two immiscible phases, and L–S = liquid and solid phases.

consequence, stress developed in the system under shear flow is borne only by LPF chains. The relaxation process then causes the shear-induced phase separation. The oligomers are squeezed by shear flow bringing about demixing due to the enhancement in the concentration fluctuation. In contrast to the system of PPPP, the system of PMPP exhibits opposite phenomena. The freezing point curve of PMPP at $\dot{\gamma}$ of 147 and 489 s⁻¹ shifts slightly toward lower temperature at a low concentration of < 2.0%, and shear flow does not significantly influence the miscibility in the case of PMPP due to the higher miscibility than PPPP. Further, if molecular orientation might be induced by the shear, PPPP aligned toward the shear flow coagulated rapidly to form the nuclei due to the entropic advantage, making the activation energy for nucleation lower. These shear effects make the homo-oligomers precipitate more rapidly than the co-oligomers, and the difference in the miscibility is amplified by the shear. As shown in Table 1, DP_n of the oligomers when the solution became turbid in the polymerization of *p*-ABA decreased gradually with the increase in $\dot{\gamma}$, and this result supports the above discussion.

Shear flow influences both reactivity of monomers and miscibility. Shear flow reduces the difference in the reactivity between *p*-ABA and *m*-ABA, bringing about the unfavorable condition for the formation of *p*-oxybenzoyl homo-oligomers. On the contrary, shear flow enhances the difference in the miscibility between homo-oligomers and co-oligomers, leading to more rapid precipitation of homo-oligomers than co-oligomers. Thus, the enhancement of fractionability was examined by tuning the application time of the shear flow. The difference in the reactivity between *p*-ABA and *m*-ABA became larger at $\dot{\gamma}$ of 0 s⁻¹ than at higher $\dot{\gamma}$. Further, *p*-oxybenzoyl homo-oligomers were precipitated more rapid under shear flow. Based on these, the polymerization was carried out without shear flow until 35 min when the precipitation started, and then the shear flow at $\dot{\gamma}$ of 147 s⁻¹ was applied after 35 min. The results are presented in Table 2 with the results with 147 s⁻¹ shear for 6 h and without shear flow for comparison. The yield was slightly decreased, but the value of χ_p became lower as shown in run no. 1. This indicates that the fractionability enhanced with the shear rate and the application period.

Table 2. Results of copolymerization of *p*-ABA with *m*-ABA^a at χ_f^b of 30 mol%

Run no.	Shear flow sequence	Polymer yield [%]	χ_p^d [mol%]
	Shear rate [s ⁻¹] x time		
1	0 x 0-35min, 147 x 35min-6h	25.0	5.2
2	0 x 6h	44.5	12.3
3	147 x 6h	29.3	8.5

^a Polymerizations were carried out in LPF at 330°C at a concentration of 1.0% for 6 h.

^b χ_f stands for the content of *m*-oxybenzoyl moiety in feed.

^c Shearing was applied from the beginning of polymerization.

^d χ_p stands for the content of *m*-oxybenzoyl moiety in the products.

CONCLUSIONS

The polymers containing few *m*-oxybenzoyl moieties were obtained as precipitates even at high χ_f in the

polymerization system of *p*-ABA and *m*-ABA under shear flow. The yield of precipitated polymers became lower with the increase in γ , but the fractionability was enhanced. Higher γ gave lower χ_p . The values of χ_p were controlled by γ . The shear flow reduced the difference on the reactivity between *p*-ABA and *m*-ABA, but made homo-oligomers more immiscible and co-oligomers slightly miscible, leading to the enhancement of the difference on the miscibility between homo-oligomers and co-oligomers. Furthermore, composition control was enabled by means of controlling shear rate and the time when introducing shear flow. This result provides a new methodology to control the composition of copolymers.

References

- (1) For examples: (a) Gentle, F. T.; Suter, U. W. *Comprehensive Polymer Science*; Allens, G., Bevington, J. C., Eds., Pergamon: New York, 1989; Vol. 5, p 97. (b) Ueda, M.; Kakuta, M.; Morozumi, T.; Sato, R. *Polym. J.* **1991**, *23*, 167. (c) Ueda, M.; Morozumi, T.; Kakuta, M. *Polym. J.* **1991**, *23*, 167. (d) Gentle, F. T.; Suter, U. W. *Makromol. Chem.* **1991**, *192*, 663. (e) Ueda, M.; Morishima, T.; Kakuta, M.; Sugiyama, J. *Macromolecules* **1992**, *25*, 6580. (f) Ueda, M.; Sugiyama, J. *Macromolecules* **1994**, *27*, 240. (g) Ueda, M.; Okada, T. *Macromolecules* **1994**, *27*, 3449. (h) Ueda, M. *J. Polym. Sci. Polym. Chem. Ed.* **2000**, *38*, 3875. (i) Ueda, M. *J. Polym. Sci. Polym. Chem. Ed.* **2000**, *38*, 2106. (j) Kameyama, A.; Murakami, Y.; Nishikubo, T. *Macromolecules* **1999**, *32*, 1407. (2) For examples: (a) Higashi, F.; Tobe, T. *Macromol. Chem. Phys.* **2001**, *202*, 745. (b) Yokozawa, T.; Asai, T.; Sugi, R.; Ishigooka, S.; Hirooka, S. *J. Am. Chem. Soc.* **2000**, *122*, 8313. (c) Yokozawa, T.; Suzuki, H. *J. Am. Chem. Soc.* **1999**, *121*, 11573. (d) Yokozawa, T.; Suzuki, Y.; Hiraoka, S. *J. Am. Chem. Soc.* **2001**, *123*, 9902. (e) Shibasaki, Y.; Arai, T.; Ueda, M. *Polym. J.* **2002**, *34*, 261. (3) For examples: (a) Akutsu, F. *J. Polym. Sci. Polym. Chem. Ed.* **1999**, *37*, 2055. (b) Hayashihara, K.; Sasaki, T.; Suzuki, M. *Polym. Prepr. Jpn.* **2000**, *49*, 152. (c) Nagahata, R. *Polym. Adv. Technol.* **2000**, *11*, 727. (d) Kameyama, A.; Kimura, K.; Nishikubo, T. *J. Polym. Sci. Polym. Chem. Ed.* **2001**, *39*, 951. (e) Nagahata, R. *J. Polym. Sci. Polym. Chem. Ed.* **2000**, *38*, 3360. (4) Zhao, D.; Moore, J. S. *J. Am. Chem. Soc.* **2003**, *125*, 16294. (5) Zhao, D.; Moore, J. S. *Org. Biomol. Chem.* **2003**, *1*, 3471. (6) Kimura, K.; Yamashita, Y. *J. Polym. Sci. Part A, Polym. Chem.* **1996**, *34*, 739. (7) Kimura, K.; Kohama, S.; Kuroda, J.; Shimizu, Y.; Ichimori, T.; Yamashita, Y. *J. Polym. Sci., Part A, Polym. Chem.* **2006**, *44*, 2732. (8) For examples: (a) Wunderlich, B. *Macromolecular Physics*; Academic Press: New York, 1973; Vol. 1. (b) Guerra, G.; Titomanlio, G. *Macromolecular Symposia*; Wiley-VCH: New York, 2002; Vol. 185. (9) Pennings, A. J.; Kiel, A. M. *Kolloid Z. Z. Polym.* **1965**, *205*, 160. (10) Pennings, A. J.; van der Mark, J. M. A. A.; Kiel, A. M. *Kolloid Z. Z. Polym.* **1970**, *237*, 336. (11) Pennings, A. J.; van der Mark, J. M.; Booij, H. C. *Kolloid Z. Z. Polym.* **1969**, *236*, 99. (12) Lovinger, A. J.; Davis, D. D. *Macromolecules* **1986**, *19*, 1861. (13) For examples: (a) Blumstein, A. *Liquid Crystalline Order in Polymers*; Academic Press: New York, 1978. (b) Donald, A.; Windle, A.; Hanna, S. *Liquid Crystalline Polymers*; Cambridge University Press: New York, 2006. (14) Cotts, D.; Berry, G. C. *Macromolecules*, **1981**, *14*, 930. (15) Agarwal, U. S.; Khakhar, D. V., *J. Chem. Phys.* **1992**, *96*, 7125. (16) Agarwal, U. S.; Khakhar, D. V. *Nature (London)* **1992**, *360*, 53. (17) Doi, M.; Edwards, S. F. *J. Chem. Soc. Faraday Trans.* **1978**, *74*, 560-918. (18) Sarker, A. K.; Kimura, K.; Yamashita, Y. *Polym. J.* **2002**, *34*, 426. (19) Kimura, K.; Kohama, S.; Kuroda, J.; Shimizu, Y.; Ichimori, T.; Yamashita, Y. *J. Polym. Sci., Part A, Polym. Chem.* **2006**, *44*, 2732. (20) Kato, Y.; Yamashita, Y.; Kimura, K.; Endo, S.; Ohta, T. *Koubunshi Ronbunshu* **1990**, *47*, 583. *Chem. Abstr.* **1990**, *113*, 116005. (21) Yamashita, Y.; Akagi, K.; Monobe, K.; Shimamura, K. *Polym. Prepr. Jpn.* **1983**, *32*, 848. (22) Richards, R. B. *Trans. Faraday Soc.* **1946**, *42*, 10. (23) Flory, P. J.; Mandelkern, L.; Hall, H. K. *J. Am. Chem. Soc.* **1951**, *73*, 2532. (24) Koningsveld, R.; Stochmayer, W. H.; Nies, E. *Polymer Phase Diagrams*; Oxford University Press: New York, 2001. (25) Krause, C.; Horst, R.; Wolf, B. A. *Macromolecules* **1997**, *30*, 890. (26) Ver Strate, G.; Phillipoff, W. *J. Polym. Sci., Polym. Lett. Ed.* **1974**, *12*, 267. (27) Schumidt, R. J.; Wolf, B. A. *Colloid Polym. Sci.* **1979**, *257*, 1188. (28) Rangel-Nafaile, C.; Metzner, A. B.; Wissbrun, K. F. *Macromolecules* **1984**, *17*, 1187. (29) Hashimoto, T.; Fujioka, K. *J. Phys. Soc. Jpn.* **1991**, *60*, 356. (30) Hashimoto, T.; Kume, T. *J. Phys. Soc. Jpn.* **1992**, *61*, 1839. (31) Kume, T.; Hattori, T.; Hashimoto, T. *Macromolecules* **1997**, *30*, 427. (32) Saito, S.; Matsuzaka, K.; Hashimoto, T. *Macromolecules* **1999**, *32*, 4879. (33) Helfand, E.; Fredrickson, G. H. *Phys. Rev. Lett.* **1989**, *62*, 2468. (34) Onuki, A. *Phys. Rev. Lett.* **1989**, *62*, 2472; *J. Phys.: Condens. Matter* **1997**, *9*, 6119. (35) Milner, S. T. *Phys. Rev. E* **1993**, *48*, 3674. (36) Doi, M.; Onuki, A. *J. Phys. II* **1992**, *2*, 1631.